Light-Scattering Studies of Styrene−(Ethylene-*co*-butylene)−Styrene Triblock Copolymer and Its Sulfonated Ionomers in Tetrahydrofuran

Chi Wu,*,† Kafai Woo,† and Ming Jiang‡

Department of Chemistry, The Chinese University of Hong Kong, Shatin, Hong Kong, and Institute of Macromolecular Science, Fudan University, Shanghai 200433, China

Received February 15, 1996; Revised Manuscript Received May 1, 1996[⊗]

ABSTRACT: A combination of static and dynamic laser light scattering (LLS) was used to study a styrene−(ethylene-*co*-butylene)−styrene triblock copolymer (SEBS) and its sulfonated ionomers in THF at 25 °C. We found that the SEBS solution unexpectedly contained a small amount of clusters whose dissolution in THF is an extremely slow process. On average, each initial SEBS aggregate contains 15−20 individual SEBS chains. As for the SEBS ionomers, the solutions contained species much larger than individual sulfonated SEBS chains. This study revealed that these large species can very slowly dissolve in THF and the dissolution process follows a first-order kinetics. Moreover, we found that the solubility of sulfonated SEBS ionomers decreased with increasing storage time even when the solids were under sealed and dry conditions. These results suggest that the origin of "association of sulfonated SEBS ionomers" should be reconsidered; namely, these large species were not formed from individual chains in solution, but instead were fragments produced in the dissolution process. In addition, the study of the complexation of sulfonated SEBS ionomers respectively with poly(styrene-*co*-4-vinylpyridine) (PSVP) and poly(methyl methacrylate-*co*-4-vinylpyridine) (PMMAVP) showed a maximum (in terms of the size or amount of the formed complexes or viscosity) at an equimolar condition, no matter what kind of metal counterions were used. This suggests a complexation mechanism different from coordination between small molecules.

Introduction

Ionomers have been extensively studied in the last two decades mainly due to their unique physical properties.[1−10] Recently, Eisenberg *et al.*[11] proposed a new morphological model for random ionomers on the basis of the existence of multiplets (aggregates made of several ion pairs) and restriction of the mobility of the polymer chains in their vicinity. Their model has reasonably explained a large body of experimental results in both dynamic mechanical and X-ray scattering studies. In this model, the thickness of the restricted mobility layer surrounding each multiplet is assumed to be of the order of the polymer chain's persistence length and the isolated multiplets act as large cross-links. At higher ion content, the overlap of the less mobile regions surrounding each multiplet leads to larger contiguous regions of restricted mobility. These regions are termed clusters when they display a distinct phase behavior.

As for block copolymer ionomers, one of most studied systems is the thermoplastic elastomer based on partially sulfonated styrene−(ethylene-*co*-butylene)−styrene (SEBS) triblock copolymers originally developed by Weiss *et al.*[12−14] The sulfonated SEBS ionomer has two different kinds of phase separation. One characterizes the triblock copolymer structure; and the other, the ionomeric structure of the multiplets. When Zn^{2+} was used as a counterion, compression-molded samples showed an ellipsoidal microstructure with a domain size of ∼12 nm, while a lamellar microstructure with a thickness of ∼7 nm was observed in the solution-cast sample. In the lamellar microstructure, the multiplet size was limited by the size of the polystyrene domains (or block). Weiss *et al.*[15] showed that for the ionic domains their X-ray results can be better described by a modified hard-sphere, interparticle interference model with an average ionic multiplet size of ∼2 nm and a closest approach distance of ∼3.5 nm. However, under identical conditions, when Zn^{2+} was replaced by Na^{+}, no lamellar structure was observed. No detailed explanation has yet been given to account for this difference between Zn-SEBS and Na-SEBS.

On the other hand, the interaction between a random ionomer and an amine- or pyridine-containing polymer has also been studied for a long time.[16−23] Peiffer *et al.*[24] showed that when blended with poly(styrene-*co*-4-vinylpyridine) (PSVP), the sulfonated ethylene−propylene terpolymer with transition metal as counterion exhibits a higher melt viscosity than a comparable blend without transition metal ions, which was attributed to the coordination between PSVP and sulfonated ionomer through transition metal ions. It was found that the stoichiometric ratio of [pyridine]/[sulfonate] or [amine]/[sulfonate], which was normally determined from the maximum in the plot of the reduced solution viscosity versus the solution blend composition, was in the range of 1−6, very much depending on the solvent and transition metal ion used. The fluorescence study indicated a proton transfer between the sulfonated group on the ionomers and the nitrogen atom on pyridine-containing polymers.[19] It has been demonstrated that the addition of small amine molecules can greatly suppress the complex formation between the sulfonated ionomer and nitrogen-containing polymers.[20]

This study of SEBS and its sulfonated ionomers originally had three objectives: (1) to find direct evidence for our previously observed intramolecular association, (2) to reveal why the solution-cast Zn-SEBS showed a different microstructure (lamellar structure) from Na-SEBS under identical experimental conditions, and (3) to determine the coordination number for the complexation between the sulfonated SEBS ionomer

† The Chinese University of Hong Kong.
‡ Fudan University.
⊗ Abstract published in *Advance ACS Abstracts,* June 15, 1996.

with different transition metal ions and vinylpyridine-containing polymer with different backbones.

Experimental Section

Sample Preparation. SEBS (courtesy of Shell Co.) contains one hydrogenated butadiene (a random copolymer of ethylene and butylene) block ($M \sim 35\,000$) and two styrene blocks ($M \sim 7500$ on each block). The blocks were made by anionic polymerization. The details of the sulfonation can be found elsewhere.[25] In this study, 70 g of SEBS was dissolved in 700 mL of 1,2-dichloroethane at 50 °C and under a nitrogen atmosphere. After the dissolution, a proper amount of freshly prepared acetyl sulfate was slowly added to the solution to sulfonate SEBS, which typically took ~2 h. The sulfonation was stopped by adding 70 mL of isopropyl alcohol. The reaction product was then divided into several portions. One was precipitated in ethanol, while the others were first neutralized with different metal acetates in ethanol and then precipitated in excess ethanol. The precipitates were repeatedly washed with boiling water to remove free acid and acetates. Such obtained precipitates were immersed in ethanol for at least 15 h. Finally, after removing ethanol, the sulfonated SEBS ionomers were dried at 50 °C under vacuum for ~1 week. Hereafter, different sulfonated SEBS are abbreviated as #-M-SEBS, where # represents the mole percentage of sulfonated groups; and M, the metal counterion used. For example, 6.9-Cu-SEBS represents a copper sulfonated SEBS with a total of 6.9 mol % ionic groups on its two polystyrene blocks.

Both poly(styrene-*co*-4-vinylpyridine) (PSVP) and poly(methyl methacrylate-*co*-4-vinylpyridine) (PMMAVP) were prepared by free-radical polymerization in THF under nitrogen protection. The amounts of vinylpyridine in PSVP and PMMAVP, which were determined by nitrogen analysis, were 13.3 and 14.8 mol %, respectively. The apparent weight-average molecular weights of PSVP and PMMAVP obtained in size exclusion chromatography (on the basis of the polystyrene calibration) were 2.38×10^4 and 2.55×10^4 g/mol, respectively.

Laser Light Scattering (LLS). The excess absolute scattered light intensities and intensity−intensity time correlation functions of the sulfonated SEBS ionomers (with six different metal counterions) with or without blending with PSVP (or PMMAVP) in THF were measured over a scattering angle range of 15−150° with a modified commercial LLS spectrometer (ALV/SP-125 equipped with an ALV-5000 multi-τ digital time correlator). A solid-state laser (ADLAS DPY425II, output power is ~400 mW at $\lambda = 532$ nm) was used as the light source. The incident beam was vertically polarized with respect to the scattering plane. The details of the LLS instrumentation and theory can be found elsewhere.[26,27] All light-scattering solutions were prepared by dissolving a proper amount of polymer(s) in THF at room temperature and then clarified by either a 0.5-μm Millipore filter or a 0.1-μm Whatman filter. All LLS measurements were done at 25.0 ± 0.1 °C.

In static LLS, for a dilute polymer solution at a relatively low scattering angle θ, the angular dependence of the excess absolute time-averaged scattered intensity, known as the excess Rayleigh ratio $R_{vv}(\theta)$, can be related to the weight-average molecular weight M_w, the second virial coefficient A_2, and the root-mean square z-average radius of the polymer chain $\langle R_g^2\rangle_z^{1/2}$ (or written as $\langle R_g\rangle$) as[28]

$$\frac{KC}{R_{vv}(\theta)} \approx \frac{1}{M_w}\left(1 + \frac{1}{3}\langle R_g^2\rangle_z q^2\right) + 2A_2C \qquad (1)$$

where $K = 4\pi(dn/dC)^2 n^2/(N_A\lambda_0^4)$ and $q = (4\pi n/\lambda_0)\sin(\theta/2)$ with N_A, dn/dC, n, and λ_0 being Avogadro's number, the specific refractive index increment, the solvent refractive index, and the wavelength of light in vacuo, respectively. After measuring $R_{vv}(\theta)$ at a set of C and θ, we were able to determine M_w, $\langle R_g\rangle$, and A_2 from a Zimm plot which incorporates θ and C extrapolation on a single grid.

In dynamic LLS, the intensity−intensity time correlation function $G^{(2)}(t,q)$ in the self-beating mode can be related to the first-order electric field time correlation function $|g^{(1)}(t,q)|$ as[26,27]

$$G^{(2)}(t,q) = \langle I(0)I(t)\rangle = A[1 + \beta|g^{(1)}(t,q)|^2] \qquad (2)$$

where A is a measured baseline; β, a parameter depending on the coherence of the detection; and t, the delay time. For a polydisperse sample, $|g^{(1)}(t,q)|$ can be related to the normalized characteristic line-width distribution $G(\Gamma)$ by

$$|g^{(1)}(t,q)| = \langle E(0)E^*(t)\rangle = \int_0^\infty G(\Gamma)\, e^{-\Gamma t}\, d\Gamma \qquad (3)$$

Using the Laplace inversion program CONTIN[29] equipped with the correlator, we were able to calculate $G(\Gamma)$ from $G^{(2)}(t,q)$ on the basis of eqs 2 and 3. In general, Γ is a function of both C and q. As C increases, the interaction between polymer molecules will affect the diffusion process. On the other hand, as q increases, the internal molecular motions will influence Γ. For a diffusive relaxation, these effects can be expressed in the form of[30,31]

$$\Gamma/q^2 = D(1 + k_d C)(1 + f\langle R_g^2\rangle q^2) \qquad (4)$$

where D is the translational diffusion coefficient at $C \to 0$ and $q \to 0$; k_d, the diffusion second virial coefficient; and f, a dimensionless number much depending on the chain conformation and internal motions. For a very dilute solution and $\langle R_g\rangle q \ll 1$ as in this study, $D \cong \Gamma/q^2$.

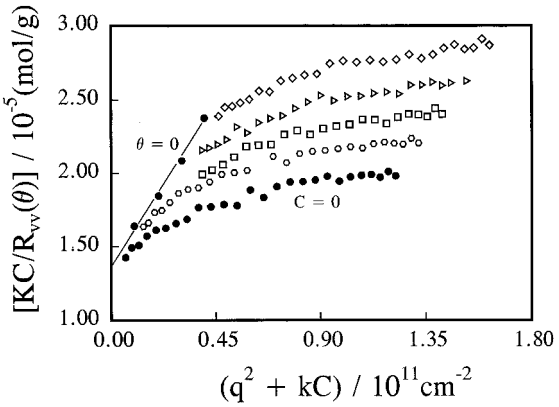

Figure 1. Typical Zimm plot for SEBS in THF at 25 °C when the solution was clarified with a 0.5-μm filter, where C ranged from 9.83×10^{-4} to 4.02×10^{-3} g/mL.

Results and Discussion

Existence of Large Clusters in SEBS. Figure 1 shows a typical Zimm plot for SEBS before its sulfonation in THF after ~14-day dissolution when the solution was clarified with a 0.5-μm filter. On the basis of eq 1, we have $M_w = 7.27 \times 10^4$ g/mol, $A_2 = 1.2 \times 10^{-3}$ mol cm^3/g^2, and $\langle R_g\rangle = 46.6$ nm respectively from the extrapolation of $[KC/R_{vv}(\theta)]_{q\to0,C\to0}$, the slopes of $[KC/R_{vv}(\theta)]_{q\to0}$ versus C, and the initial slope of $[KC/R_{vv}(\theta)\}_{C\to0}$ versus q^2. It should be noted that these are apparent values because we have not taken into account the contribution from refractive index increments of each block to the scattering intensity. The positive value of A_2 indicates that THF is a good solvent for SEBS at 25 °C. However, the curvature of $KC/R_{vv}(\theta)$ versus q^2 and the higher values of M_w and $\langle R_g\rangle$ are unexpected since SEBS has a known molar mass of ~5 × 10^4 and its chain size should be ~10 nm. Further dynamic LLS study revealed the existence of a small amount of larger clusters in SEBS even after ~14-day dissolution in a good solvent.

Figure 2 shows a normalized intensity−intensity time correlation function $[g^{(2)}(t,q) - A]/A$ for SEBS in THF

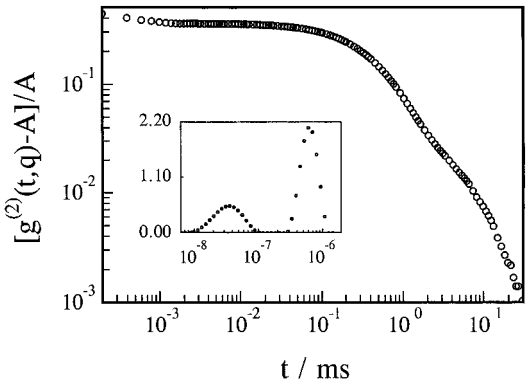

Figure 2. Normalized intensity−intensity time correlation function $[g^{(2)}(t,q) - A]/A$ for SEBS in THF after ~14-day dissolution, where the solution was clarified with a 0.5-μm filter. The insert shows an apparent translational diffusion coefficient distribution $G(\Gamma/q^2)$ calculated from a Laplace inversion of $[g^{(2)}(t,q) - A]/A$.

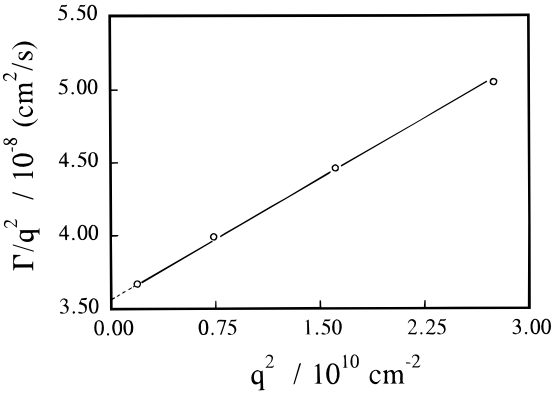

Figure 3. Typical q^2 dependence of the average line width $\langle\Gamma\rangle_{slow}/q^2$ for the slow relaxation process in Figure 2, where $C = 9.83 \times 10^{-4}$ g/mL.

after ~14-day dissolution when the solution was clarified with a 0.5-μm filter. The insert in Figure 2 shows an apparent translational diffusion coefficient distribution $G(\Gamma/q^2)$ calculated from a Laplace inversion of $[g^{(2)}(t,q) - A]/A$ on the basis of eqs 2 and 3. Two distinct relaxation processes are evident in both $[g^{(2)}(t,q) - A]/A$ and $G(\Gamma/q^2)$. The fast relaxation process is attributed to the translational diffusion of individual SEBS chains.

Figure 3 shows a typical q^2 dependence of the average line width $\langle\Gamma\rangle_{slow}/q^2$ for the slow relaxation process in Figure 2, where $C = 9.83 \times 10^{-4}$ g/mL. The fact that $\langle\Gamma\rangle_{slow}/q^2$ is linearly dependent on q^2 indicates that the slow relaxation can be related to the translational diffusion of some larger and slow-moving species, possibly some unexpected SEBS clusters. As for the fast relaxation process, $\langle\Gamma\rangle_{fast}/q^2$ is a constant at different scattering angles. Our study also showed that both relaxation processes in Figure 2 are linearly, but weakly, dependent on the SEBS concentration, and the value of k_d estimated on the basis of eq 4 is in the range of 10−20 mL/g. Therefore, in our studied concentration range (9.83×10^{-4} to 4.02×10^{-3} g/mL), the concentration correction of $\langle\Gamma\rangle$ is only a few percent. Using a recently proven method of combining M_w from static LLS and the area ratio (A_r) of the two peaks in $G(\Gamma/q^2)$ from dynamic LLS,[32] we estimated that on average each SEBS cluster contains ~15−20 SEBS chains and the weight percentage of large clusters is ~3%, so that the number percentage should be less than 0.2%. Heating the SEBS solution to ~60 °C did not help to dissolve the large SEBS clusters. On the other hand, we

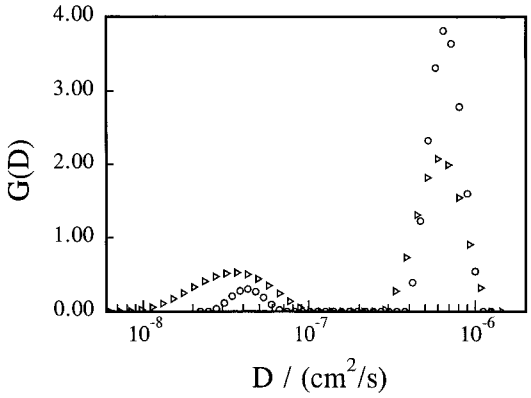

Figure 4. Dissolution time dependence of the translational diffusion coefficient distribution $G(D)$, where "△" represents the freshly prepared SEBS in THF; and "○", the same solution after ~1 year.

Table 1. Summary of the Static LLS Results for SEBS in THF at 25 °C

				$\langle R_h\rangle$/nm	
filter	t_{meas}	$M_w/10^4$	$\langle R_g\rangle$/nm	SEBS	cluster
0.5 μm	after dust-free	7.27	47	~13	~120
	after 1 year	5.20	18	~13	~110
0.1 μm	after dust-free	4.89	~13	~13	

discovered that they could very slowly dissolve in THF at room temperature.

Figure 4 shows a dissolution time dependence of the translational diffusion coefficient distribution $G(D)$ for SEBS in THF at 25 °C. The peak area corresponding to the SEBS clusters became smaller after ~1 year, while the peak area related to individual SEBS chains became larger at the same time, which indicates a slow dissolution of the SEBS clusters. Static LLS study also shows that after ~1 year the curvature in Figure 1 disappeared and both M_w and $\langle R_g\rangle$ decreased with increasing time. Later, we found that the SEBS clusters could be removed by a 0.1-μm filter, and only a single narrowly distributed peak corresponding to individual SEBS chains was observed in $G(D)$.

Table 1 summarizes both static and dynamic LLS results for SEBS in THF at 25 °C, where the values of $\langle R_h\rangle$ were calculated on the basis of the Stokes−Einstein equation: $\langle R_h\rangle = k_BT/(6\pi\eta\langle D\rangle)$, with k_B and η being the Boltzmann constant and solvent viscosity, respectively. Table 1 shows that using a 0.1-μm filter we were able to determine molecular parameters for individual SEBS chains in THF. The existence of these large SEBS clusters has been overlooked in previous studies. One speculation for the large SEBS clusters is that they were formed through possible crystallization of the middle EB block if the E and B blocks were not as random as we thought. The exact nature of the SEBS clusters is still unknown, but it is important to remove them before further studies of sulfonated SEBS ionomers.

"Association" of Sulfonated SEBS Ionomers in THF. Figure 5 shows a typical differential distribution $F(R_h)$ of apparent hydrodynamic radius for 6.9-Ni-SEBS in THF, where $C = 1.59 \times 10^{-4}$ g/mL. $F(R_h)$, defined as $G(\Gamma)\Gamma(\Gamma/q^2)(6\pi\eta)/(k_BT)$, was calculated from $G(\Gamma)$, where we used $\Gamma/q^2 \cong D = (k_BT)/(6\pi\eta R_h)$.[33] For 6.9-Ni-SEBS in THF, $F(R_h)$ has two incompletely merged peaks. A comparison with the $F(R_h)$ for SEBS clearly shows that for 6.9-Ni-SEBS the peak with a larger average R_h can be attributed to the clusters of sulfonated SEBS chains, while the peak with a smaller average R_h indicates a possible intramolecular associa-

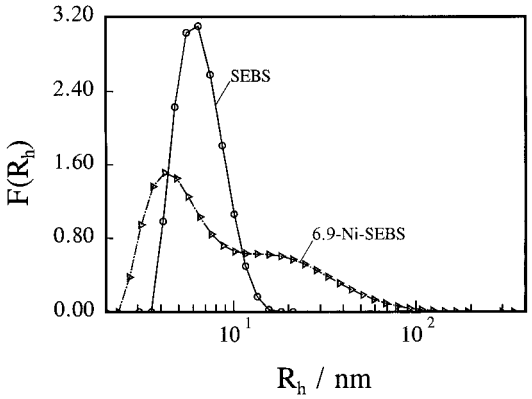

Figure 5. Typical differential distribution $F(R_h)$ of apparent hydrodynamic radius for 6.9-Ni-SEBS in THF at 25 °C, where $C = 1.59 \times 10^{-4}$ g/mL. $F(R_h)$ for SEBS without the sulfonation is plotted for comparison.

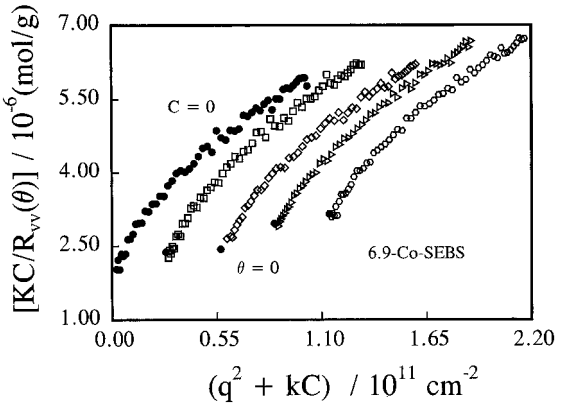

Figure 6. Typical Zimm plot for 6.9-Co-SEBS in THF after ~100-h dissolution at 25 °C, where C ranged from 1.13×10^{-4} to 4.52×10^{-4} g/mL and the solutions were clarified with a 0.5-μm filter.

tion, which reduces the hydrodynamic volume of the polymer chain. This intramolecular interaction was observed before; namely, in a very dilute solution, the intrinsic viscosity of 6.9-Ni-SEBS in THF is lower than that of SEBS under identical conditions.[34] Figure 5 provide direct evidence that the intramolecular interaction (association) can reduce the chain dimension of sulfonated SEBS ionomers.

Figure 6 shows a typical Zimm plot for 6.9-Co-SEBS in THF after ~100-h dissolution at room temperature, where C ranged from 1.13×10^{-4} to 4.52×10^{-4} g/mL and the solutions were clarified with a 0.5-μm filter. The positive value of A_2 shows that THF is also a good solvent for 6.9-Co-SEBS. On the other hand, the curvature and high value of $M_w = 4.82 \times 10^5$ g/mol clearly indicate the existence of some species larger than individual sulfonated SEBS chains. The values of M_w measured for all metal counterions studied were much higher than that of individual sulfonated SEBS chains. Further studies showed that these large species could slowly dissolve in THF at room temperature and the speed of the dissolution process and the final size of the larger species were very much dependent on the metal counterion used.

Figure 7 shows a typical dissolution time dependence of the weight-average molar mass (M_w) of 6.9-Co-sulfonated SEBS. M_w levels off when $t > 600$ h. In addition, we also observed that the curvature in the Zimm plot gradually disappeared and $\langle R_g \rangle$ decreased from 92 to 22 nm. Our static LLS results clearly showed the slow dissolution of the large species. Similar

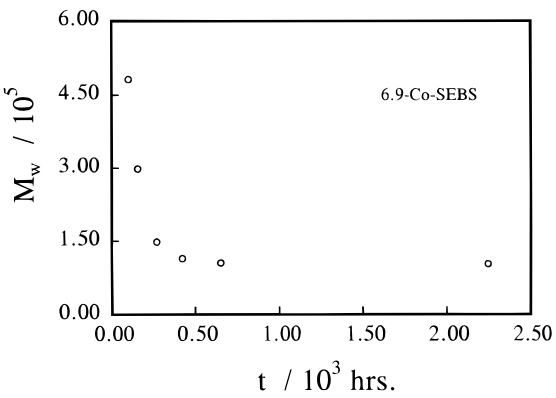

Figure 7. Typical dissolution time dependence of the weight-average molar mass (M_w) for 6.9-Co-SEBS in THF at 25 °C.

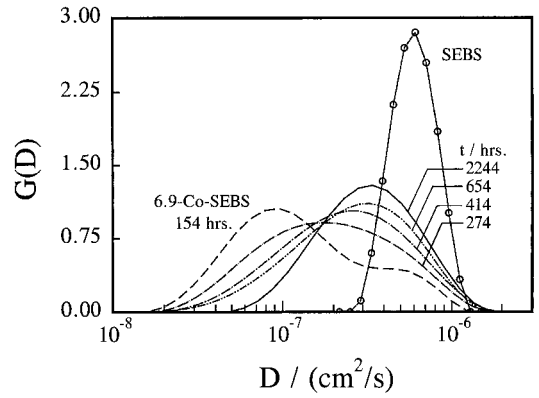

Figure 8. Typical dissolution time dependence of the translational diffusion coeffcient distribution $G(D)$ of 6.9-Co-SEBS in THF at 25 °C, where the solution was clarified by a 0.5-μm filter and the $G(D)$ of SEBS in THF is plotted for comparison.

behavior was also observed for sulfonated SEBS ionomers with other metal counterions, such as Ni-SEBS, Cu-SEBS, Mn-SEBS, Zn-SEBS, and Na-SEBS. The fact that these large species were able to slowly dissolve in THF suggests that they were not formed *in the solution* through the association of individual 6.9-Co-SEBS chains, but instead they were formed *in the bulk* before its dissolution in THF because if these large species were formed in the solution through some kind of intermolecular interactions (associations), it would be difficult to explain why they were able to slowly dissolve again in the same solution under the same conditions. This extremely slow dissolution can be better viewed in dynamic LLS.

Figure 8 shows a typical dissolution time dependence of the translational diffusion coefficient distribution $G(D)$ for 6.9-Co-SEBS in THF at 25 °C, where the solution was clarified by a 0.5-μm filter and the $G(D)$ for SEBS in THF was also plotted for comparison. At $t \sim 154$ h, $G(D)$ has two incompletely merged peaks. One peak located at the same position as that of SEBS obviously represents individual 6.9-Co-SEBS chains; the other broad peak located at a lower D can be attributed to species which have not dissolved. After a long dissolving time, the two peaks merged into one broad peak and the peak position gradually moved toward a higher D, i.e., a smaller hydrodynamic size. As stated before, the average hydrodynamic radius can be calculated from $G(D)$ by replacing D with $\langle D \rangle$ in the Stokes–Einstein equation.

Figure 9 shows a semilogarithmic plot of $\Delta\langle R_h \rangle$ versus t for 6.9-Co-SEBS in THF at 25 °C, where t is the dissolution time and $\Delta\langle R_h \rangle$ [$=\langle R_h \rangle_t - \langle R_h \rangle_\infty$] is the

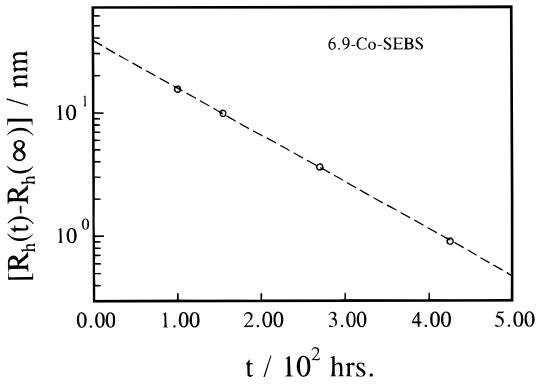

Figure 9. Semilogarithmic plot of $\Delta\langle R_h\rangle$ versus t for 6.9-Co-SEBS in THF at 25 °C, where t is the dissolution time and $\Delta\langle R_h\rangle$ [$=\langle R_h\rangle_t - \langle R_h\rangle_\infty$] is the difference between the average hydrodynamic radius at time t and infinity.

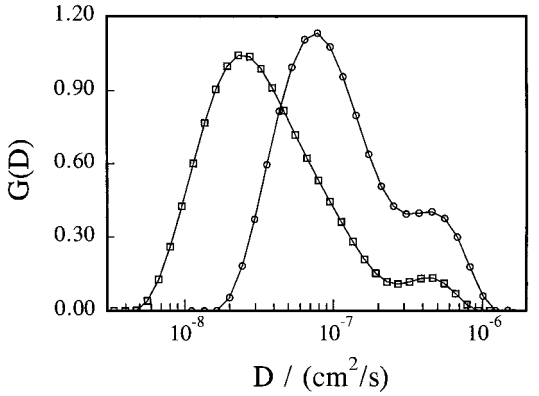

Figure 10. Time dependence of the line-width distribution $G(\Gamma/q^2)$ for 6.9-Mn-SEBS in THF, where $C = 4.88 \times 10^{-4}$ g/mL: (○) the solution was prepared from a newly made sample; and (□) the solution was prepared ~1 year later from the same solid sample which was stored under sealed and dry conditions.

difference between the average hydrodynamic radius at time t and ∞. Practically, we determined $\langle R_h\rangle_\infty$ after a very long dissolution time (~3−6 months). The line represents a least-squares fitting of $\log(\Delta\langle R_h\rangle) = 1.58 - 3.84 \times 10^{-3}t$ or $\Delta\langle R_h\rangle = 38.3 \exp(-t/\tau)$ with $\tau = 113$ h, which shows that the dissolution process follows a first-order kinetics. Our results showed that for different metal counterions, τ increased considerably from ~10^2 to ~10^3 h in the order $Mn^{2+} \sim Na^+ > Cu^{2+} \sim Ni^{2+} \sim Zn^{2+} > Co^{2+}$.

Figure 10 shows a sample storage time dependence of $G(D)$ for 6.9-Mn-SEBS in THF at 25 °C. After the bulk 6.9-Mn-SEBS was stored for ~1 year under sealed and dry conditions, the peak (with a larger D) representing individual 6.9-Mn-SEBS chains became smaller, while the peak representing larger species shifted to a lower D and at the same time the peak area increased, which implies that after ~1 year the large species became even larger and more large species were formed through the association of individual 6.9-Mn-SEBS chains in the bulk. For all metal counterions studied, we found that the longer the storage time, the more difficult their dissolution in THF will be. In the case of Mg^{2+}, after 1 year of storage, 6.9-Mg-SEBS was only able to swell in THF. The nature of this unexpected association in bulk remains unknown at this time.

Figure 11 shows a schematic of the dissolution process. In bulk, a three-dimensional network was formed through the linkage of individual sulfonated SEBS chains with the linking point being the ion-pair multiplets formed between the sulfonated styrene blocks. If the linkage of these ion-pair multiplets is strong, such as in the case of Mg^{2+}, the network will be swollen by a good solvent, such as THF, but not be dissolved. If the linkage is not that strong, but not too weak, the network will break into many small microgels, such as in the cases of Mn^{2+} and Na^+. These small microgels were often mistaken as the "association" of individual polymer chains *in the solution*. For a weak linkage, such as in the cases of Ni^{2+}, Zn^{2+}, and Cu^{2+}, these small microgels will further break into some "star-like" clusters. In this case, the swelling stress existing inside the microgel networks is greatly reduced. For an even weaker linkage, such as in the case of Co^{2+}, these starlike clusters will eventually break into "trimers or dimers" or even individual polymer chains.

On the basis of our results and proposed dissolution process, the observed microstructure difference between the solution-cast Zn-SEBS and Na-SEBS is explainable. In the case of Zn-SEBS, the linkage is weaker so that its dissolution ends up with some starlike clusters with $\langle R_h\rangle \sim 12$ nm. These starlike clusters act as the building blocks to form a lamellar structure with a thickness of ~12 nm during the casting process, while in the case of Na-SEBS, the linkage is much stronger so that the solution finally only contains microgels with $\langle R_h\rangle \sim 30$ nm. In the casting process, these microgels can only pack randomly together so that no lamellar structure can form. On the basis of the above discussion, we here speculate a dissolution time dependence of the microstructure in the solution-cast Zn-SEBS samples. Further X-ray studies have been planned to verify this point.

Complexation between Sulfonated SEBS with PSVP or PMMAVP. Figure 12 shows a typical composition dependence of the hydrodynamic radius distribution $F(R_h)$ for a solution blend of 6.9-Ni-SEBS and PSVP in THF, where the total concentration of 6.9-Ni-SEBS + PSVP is fixed at 1.0×10^{-4} g/mL. It clearly shows the existence of complexation between 6.9-Ni-SEBS and PSVP because the peak position shifts to a higher R_h with increasing amount of 6.9-Ni-SEBS. When the weight percent of 6.9-Ni-SEBS is higher than 60%, the average hydrodynamic radius of the solution blend is larger than that of either PSVP or 6.9-Ni-SEBS alone in THF. For the other metal counterions studied, the tendency is the same and there exists a maximum in the plot of $\langle R_h\rangle$ versus the composition of sulfonated SEBS ionomers. The viscosity measurements of these solution blends also showed a similar pattern.

Figure 13 summarizes the viscosity results, where $[\eta]_{red}$ is the reduced viscosity defined as $(\eta_{solution}/\eta_{solvent} - 1)/C$, and N_{M-SEBS} and N_{**-VP} are the numbers of #-M-SEBS and **-VP (** = PS or PMMA) chains, respectively. It should be noted that in previous studies the x axis was normally plotted as the number ratio of the two functional groups, namely [sulfonate]/[VP]. However, we have chosen to use the number ratio of the two polymer chains. It is interesting and exciting to find that for seven different kinds of metal counterions and two different kinds of VP-containing polymers the maximum reduced viscosity always appears at equimolar ratio, $N_{\#-M-SEBS}/(N_{\#-M-SEBS} + N_{**-VP}) = 0.5$, or, in other words, $N_{\#-M-SEBS}/N_{**-VP} = 1$. It should be noted that the maximum composition in Figure 13 differs from that in Figure 12 because the composition expressions are different. Figure 13 leads us to believe that when two polymer coils (A and B, for example) approach

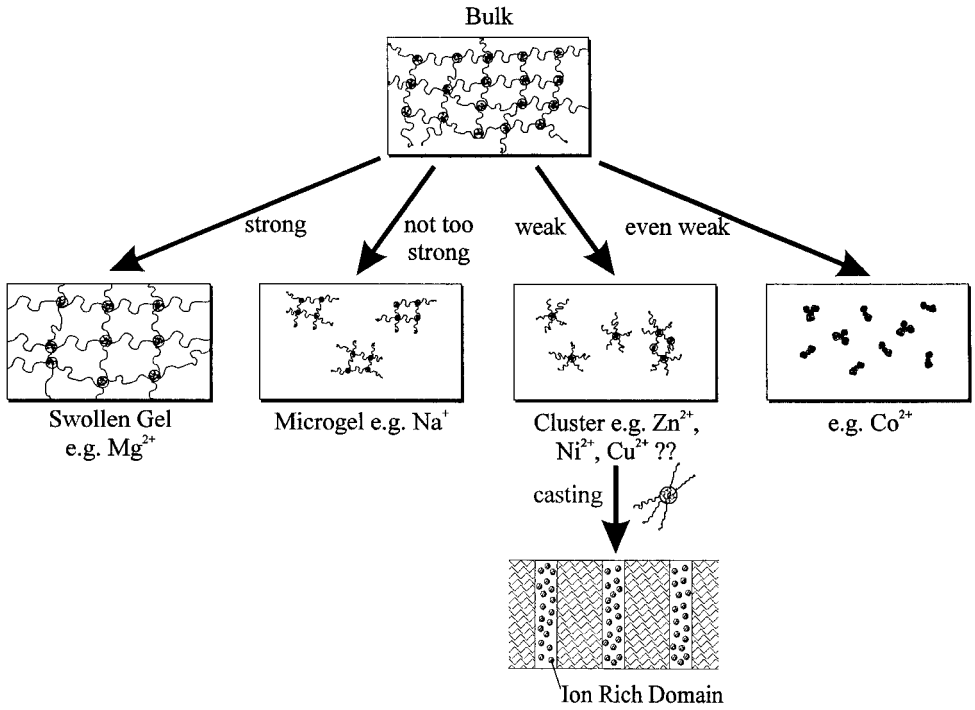

Figure 11. Schematic of the dissolution process proposed on the basis of the values of M_w, R_g, and R_h for sulfonated SEBS ionomers in THF at room temperature.

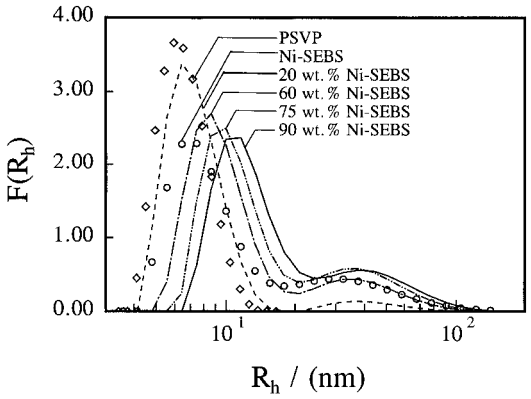

Figure 12. Typical composition dependence of the hydrodynamic radius distribution $F(R_h)$ for a solution blend of 6.9-Ni-SEBS and PSVP in THF at 25 °C, where the total concentration of 6.9-Ni-SEBS + PSVP was fixed at 1.0×10^{-4} g/mL.

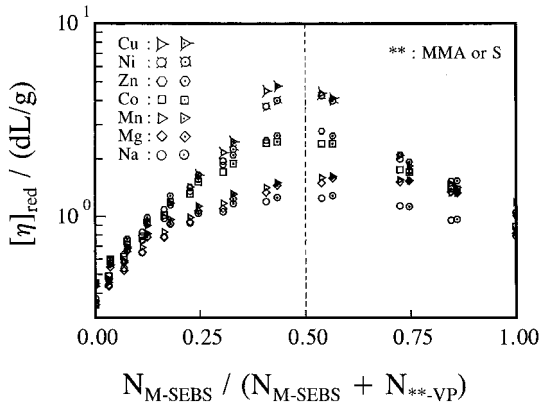

Figure 13. Plot of $[\eta]_{red}$ vs the number ratio $N_{M-SEBS}/(N_{M-SEBS} + N_{**-VP})$, where $[\eta]_{red}$ is defined as $(\eta_{solution}/\eta_{solvent} - 1)/C$ and N_{M-SEBS} and N_{**-VP} are the numbers of M-SEBS and **-VP (** = PS or PMMA) chains, respectively. The total concentration of M-SEBS and PSVP (or PMMAVP) was fixed at 1.0×10^{-2} g/mL.

together to form a complex, on average, one half surface of each coil was complexed ("covered") by another coil, such as AB or BA. If A and B are equimolar, this process can continue to form ...ABABAB... with a larger size which leads to a higher solution viscosity and a larger hydrodynamic radius. If A and B are not equimolar, it will end up with ABAB...ABA or BABA-...BAB and the size of the complex will be limited, so that the solution viscosity is lower. Literally, this complexation is like a "polycondensation".

Conclusions

Our laser light-scattering studies of a triblock copolymer, styrene−(ethylene-*co*-butylene)−styrene (SEBS), and its sulfonated ionomers showed that (1) SEBS contains ~3 wt % of large species (possibly caused by inhomogeneities in the EB block) which are practically insoluble in THF at room temperature. It should be noted that in future studies of the solution properties of SEBS or similar systems, these larger insoluble species have to be removed to ensure that individual polymer chains are studied. (2) For sulfonated SEBS ionomers in THF, the observed very large species *were not formed in the solution* through the *association* (aggregation) of individual sulfonated SEBS ionomer chains; instead they are small "insoluble" microfragments remaining in the dissolution process. These fragments can be microgels, "starlike" clusters, or even trimers and dimers, depending on the strength of the ion-pair clusters formed in the bulk. According to the solubility of their corresponding sulfonated SEBS, the strength of the ion-pair clusters is in the order $Mg^{2+} > Na^{+} \sim Mn^{2+} > Zn^{2+} \sim Cu^{2+} \sim Ni^{2+} > Co^{2+}$. The observed slow dissolution of these larger species suggests that *the origin of the association of block ionomers in solution* should be reconsidered, because if these large species were formed in solution through intermolecular interactions (associations), it would be difficult to explain why they were able to slowly dissolve again in the same solution under the same conditions. (3) The maximum reduced viscosity of the solution blends made

of sulfonated SEBS ionomers and vinylpyridine-containing polymers always appears at the equimolar point in terms of the chain number of sulfonated SEBS ionomer and vinylpyridine-containing polymer, no matter what kind of metal ion or VP-containing polymer was used, which leads us to think that on average each sulfonated SEBS chain is associated with one VP-containing polymer chain.

Acknowledgment. Financial support of this work by RGC (Research Grants Council of the Hong Kong Government) Earmarked Grants 1994/95 (CUHK A/C No. 221600460) is gratefully acknowledged. M.J. would like to thank the National Natural Science Foundation of China (NNSFC) for financial support.

References and Notes

(1) Lundberg, R. D.; Makowski, H. S. *J. Polym. Sci., Polym. Phys. Ed.* **1980**, *18*, 1821.
(2) Lantman, C. W.; MacKnight, W. J.; Lundberg, R. D. *Comprehensive Polymer Science*; Pergamon Press: New York, 1988; Vol. 2, Chapter 25, pp 755−773.
(3) Pineri, M.; Eisenberg, A. *Structure and Properties of Ionomers*; Reidel: Dordrecht, 1987; p 453.
(4) Broze, G.; Jerome, R.; Teyssie, P.; Marc, C. *Macromolecules* **1983**, *16*, 996.
(5) Lee, D.; Register, R. A.; Yang, C.; Cooper, S. L. *Macromolecules* **1988**, *21*, 998.
(6) Williams, C. E.; Russell, T. P.; Jerome, R.; Horrion, J. *Macromolecules* **1986**, *19*, 2877.
(7) Holliday, L., Ed. *Ionic Polymers*; Applied Science Publishers: London, 1975.
(8) Eisenberg, A.; King, M. *Ion-Containing Polymers, Physical Properties and Structure*; Academic Press: New York, 1977.
(9) Mauritz, K. A. *J. Macromol. Sci., Rev. Macromol. Chem. Phys.* **1988**, *C28*, 65.
(10) Wilson, A. D.; Prosser, H. J., Eds. *Developments in Ionic Polymers*; Applied Science Publishers: New York, 1983; Vols. 1, 2.
(11) Eisenberg, A.; Hird, B.; Moore, R. B. *Macromolecules* **1990**, *23*, 4098.
(12) Weiss, R. A.; Lefelar, J. A. *Polymer* **1986**, *27*, 3.
(13) Weiss, R. A.; Sen, A.; Willis, C. L.; Pottick, L. A. *Polymer* **1991**, *32*, 1867, 2785.
(14) Lu, X.; Steckle, W. P.; Weiss, R. A. *Macromolecules* **1993**, *26*, 5876, 6525.
(15) Weiss, R. A.; Sen, A.; Pottick, L. A. *Polym. Commun.* **1990**, *31*, 223.
(16) Lundberg, R.; Phillips, R.; Peiffer, D. *J. Polym. Sci., Polym. Lett. Ed.* **1989**, *27*, 245.
(17) Lu, X.; Weiss, R. *Macromolecules* **1991**, *24*, 5763.
(18) Cook, R.; King, H., Jr.; Peiffer, G. *Macromolecules* **1992**, *25*, 629.
(19) Beeker, K.; MacKnight, W. J. *Macromolecules* **1991**, *24*, 4575.
(20) Wang, J.; Peiffer, D.; Shuely, W.; Chu, B. *Macromolecules* **1991**, *24*, 4349.
(21) Agnew, N. *J. Polym. Sci., Polym. Chem. Ed.* **1976**, *14*, 2819.
(22) Belfione, H.; Graham, E.; Veda, Y. *Polym. Int.* **1992**, *28*, 81.
(23) Tsuchida, E.; Abe, K. *Adv. Polym. Sci.* **1982**, *45*, 1.
(24) Peiffer, D.; Agawal, G.; Lundberg, R. *J. Polym. Sci., Polym. Lett. Ed.* **1986**, *24*, 5817.
(25) Makowski, H.; Lundburg, R.; Signal, G. U.S. Patent 3,870,-841, 1975.
(26) Chu, B. *Laser Light Scattering*, 2nd ed.; Academic Press: New York, 1974.
(27) Pecora, R.; Berne, B. J. *Dynamic Light Scattering*; Plenum Press: New York, 1976.
(28) Zimm, B. H. *J. Chem. Phys.* **1948**, *16*, 1099.
(29) Provencher, S. W. *Biophys. J.* **1976**, *16*, 29; *J. Chem. Phys.* **1976**, *64(7)*, 2772.
(30) Stockmayer, W. H.; Schmidt, M. *Pure Appl. Chem.* **1982**, *54*, 407.
(31) Stockmayer, W. H.; Schmidt, M. *Macromolecules* **1984**, *17*, 509.
(32) Wu, C.; Siddiq, M.; Woo, K. F. *Macromolecules* **1995**, *28*, 4914.
(33) Wu, C. *Colloid Polym. Sci.* **1993**, *271*, 947.
(34) Jiang, M.; Liu, W. F. *Macromolecules*, submitted for publication.

MA960247+